BEAM INSTRUMENTATION WORKSHOP 2002

Tenth Workshop

Upton, New York 6–9 May 2002

EDITORS
Gary A. Smith
Thomas Russo
Brookhaven National Laboratory
Upton, New York

SPONSORING ORGANIZATION
Collider-Accelerator Department,
Brookhaven National Laboratory

CD-ROM INCLUDED

AMERICAN INSTITUTE OF PHYSICS

Melville, New York, 2002
AIP CONFERENCE PROCEEDINGS ■ VOLUME 648

DISCLAIMER

Laser-Compton Scattering as a Potential Electron Beam Monitor

K. Chouffani[1,*], D. Wells[1], F. Harmon[1], G. Lancaster[2], J. Jones[2]

[1]*Idaho Accelerator Center, 1500 Alvin Ricken DR., Pocatello, ID 83209, USA*
[2]*Idaho National Engineering and Environmental Laboratory, P.O. Box 1625, MS 2802, Idaho Falls, ID 83415-2802, USA*

Abstract. LCS experiments were carried out at the Idaho Accelerator Center (IAC); sharp monochromatic x-ray lines were observed. These are produced using the so-called inverse Compton effect, whereby optical laser photons are collided with a relativistic electron beam. The back-scattered photons are then kinematically boosted to keV x-ray energies. We have first demonstrated these beams using a 20 MeV electron beam collided with a 100 MW, 7 ns Nd:YAG laser. We observed narrow LCS x-ray spectral peaks resulting from the interaction of the electron beam with the Nd:YAG laser second harmonic (532 nm). The LCS x-ray energy lines and energy deviations were measured as a function of the electron beam energy and energy-spread respectively. The results showed good agreement with the predicted values. LCS could provide an excellent probe of electron beam energy, energy spread, transverse and longitudinal distribution and direction.

1 INTRODUCTION

Laser-Compton scattering (LCS) was originally viewed as a potential bright and tunable short pulse x-ray source. Recent results and publications have shown that LCS can also be used for beam diagnostics and have proved to be excellent tools to measure the electron beam divergence, longitudinal electron bunch distribution and electron beam spot sizes as small as 10 nm [1,2]. LCS is the exchange of energy between relativistic electron and laser beams. When photons interact with high energy moving electrons (in the MeV region), the electrons scatter low energy photons to a higher energy at the expense of the electrons' kinetic energy. This interaction results in the emission of highly directed (peaked in the direction of the incident electron beam), mono-energetic (see below), highly polarized and tunable x-ray beams with a divergence on the order of $1/\gamma$, where γ is the energy of the electrons relative to the electron rest energy. LCS experimental observations of bright photons generated by backscattered laser photons from relativistic electrons were reported in literature [3-5] and more recently by K. Chouffani et al. [6].

2 KINEMATICS OF LCS

Figure 1 shows a schematic illustration of LCS geometry. When an incoming photon strikes an electron of energy E_B and velocity β with a relative angle α, the

* Corresponding author. Tel:1-208-282-5874; Fax:1-208-282-5878.
E-mail address: khalid@physics.isu.edu (K. Chouffani)

CP648, *Beam Instrumentation Workshop 2002: Tenth Workshop*, edited by G. A. Smith and T. Russo

energy of the scattered photon in the plane of incidence (defined by the electron beam and incoming photon directions) is given by:

$$E_\gamma = \frac{E_L(1+\beta\cos\alpha)}{1-\beta\cos\theta + E_L(1+\cos(\alpha-\theta))/E_B} \quad (1).$$

E_γ and E_L are the photon and laser quantum energy respectively, E_B is the electron beam energy, α and θ are the angle between the laser and electron beam and emission angle respectively. LCS can occur at any

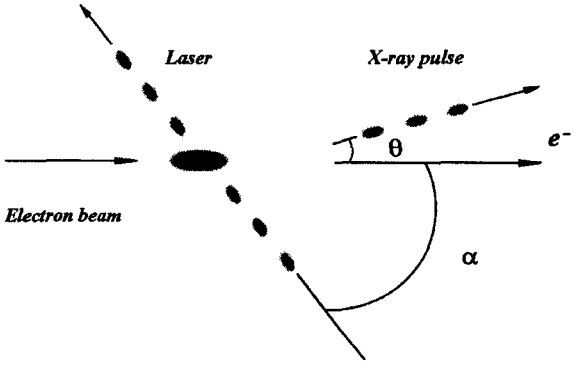

Figure 1. Laser Compton scattering (LCS) mechanism.

crossing angle between the electron and laser beam; however, two basic configurations are typically used in LCS. Head-on collision where the laser photon acquires the highest gain in energy (most energy efficient geometry). In this geometry, the x-ray pulse duration τ_x is determined primarily by the electron bunch length τ_b [5] and is given by $\tau_x = \tau_b + \tau_{Laser}/4\gamma^2$, where τ_{Laser} is the laser pulse length. In this configuration the photon energy is given by:

$$E_\gamma \approx \frac{4\gamma^2 E_L}{1+\gamma^2\theta^2 + 4E_L E_B/m^2c^4} \quad (2),$$

where m is the electron mass and c is the speed of light. The maximum photon energy occurs for $\theta = 0$ and is equal to $E_\gamma^{Max} \approx 4\gamma^2 E_L$. The other configuration is the 90° geometry where the electron beam and laser beam are orthogonal to each other. In our experiments the 90° geometry was not attempted and we will discuss only data taken from the head-on collisions. LCS spectra, when summed over θ, are relatively broad, with a range of energy of $\Delta E_\gamma/E_\gamma \leq 1$. The spectral width is limited by the electron beam emittance and energy spread [7]. Monochromaticity can, however, be achieved by collimating the forward directed x-ray beam, i.e. decreasing the detector solid angle. This will confine the LCS x-rays into a narrow energy window ranging from a cut-off energy $E_\gamma^{cut\text{-}off}$ to E_γ^{Max}.

3 EXPERIMENT

The laser-Compton scattering experiments were carried out at the Idaho Accelerator Center (IAC). The 1.3 GHz RF linac produces a 20-22 MeV electron beam that is brought to a head-on collision with a pulsed 7 ns long, 10 Hz repetition rate and 100 MW peak power Nd:YAG laser. The Nd:YAG laser fundamental wavelength is equal to 1064 nm and the second harmonic is equal to 532 nm. Interaction with a 20 MeV electron beam generates two x-ray lines at 7.5 and 15 keV, respectively, when the observation direction coincide with the electron beam direction. The laser-pulse energies of 1064 and 532 were 750 and 250 mJ respectively. During the experiment, the electron macrobunch length was varied between 2 and 20 ns and the electron bunch charge ranged from 1.4 to 8nC. A pair of slits located between two 22.5° bending magnets [6] enabled us to change the electron beam energy distribution as well as the electron beam current. The electron beam spot size and emittance were determined from optical transition radiation (OTR) measurements. During the OTR measurements, the electron beam slits were open to a maximum ($\approx$ 5 cm). The electron beam angular spread was consistent with the previous measurements made by Fiorito on the same LINAC [6,8].

Figure 2 shows the experimental and optical setup. The 9 mm diameter Nd:YAG laser beam is first expanded to a 45 mm diameter beam and then focused by a 5 m focal lens. The lens focal point coincides with the center of the interaction chamber. An off axis 45° broadband mirror, whose center is located 2.4 cm from the beam line axis, steers the laser beam toward the center of the interaction chamber. The laser beam spot size was equal to 0.12 mm for the 532 nm lines. The HeNe laser on the optics table follows the same path as the Nd:YAG laser, it used only for alignment purposes. Two fluorescent screens were placed on motorized actuators, one located at the center of the interaction chamber and the other positioned 38.1 cm upstream, to enable the LINAC operator to position the electron beam along their axis. The centers of the fluorescent screens were aligned when they were intercepted by another HeNe laser collinear with the electron beam's drift-line axis. The angle between the Nd:YAG laser beam and the beam line axis was equal to 4.65 mrad. The angle between the laser-beam and electron beam was 1.6 mrad (see below).

The x-rays from the LCS passed through a 51 μm thick Kapton window and traveled 1.8 m in air before reaching the liquid nitrogen cooled high resolution Si(Li) detector placed at 0° with respect to the beam line axis. The distance between the center of the interaction chamber and detector was equal to 6.83 m, and the solid angle sustended by the detector was about 0.68 μsr.

A scintillator coupled to a photomultiplier (PMT) tube was placed closed to the x-ray detector in order to monitor the bremsstrahlung background during beam tuning. A fast photomutiplier positioned on the optics table and a fast electron beam toroid placed at the exit of the 45° bending magnet were used for timing purposes.

The lowest acceptable bremsstrahlung signal recorded was obtained when the angle between the electron beam and the beam line axis was approximately 3mrad. The electron beam was focused on the first actuator (upstream from the interaction chamber) and the laser beam was steered toward its center. At this position the laser beam spot size is approximately 3.4 mm. From this interaction geometry, the crossing

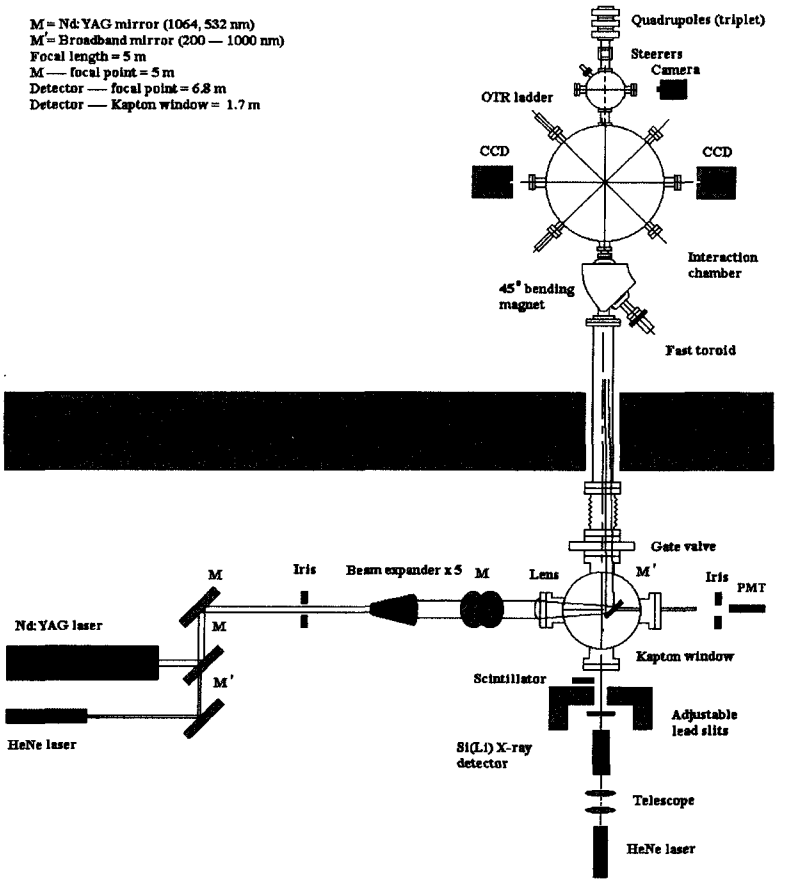

Figure 2. LCS experimental setup.

angle was of the order of 1.6 mrad. The energy calibration of the Si-(Li) detector was determined by x-ray fluorescence from the bremsstrahlung x-ray beam hitting a 343 μm thick Zr target. The detector energy resolution both with and without linac operation was determined by measuring the widths of the x-ray peaks from calibrated radioactive sources, and the bremsstrahlung induced Zr k_α x-ray emission line. The LINAC-on resolution is given by:

$$\Gamma^2_{fwhm} = 0.03956 + 0.00262 E_\gamma \quad (3),$$

where Γ_{fwhm} is the x-ray fwhm in keV, and E_γ is the x-ray energy in keV. The contribution from the RF noise was found to be small. For E_γ = 15 keV and E_γ = 7.5 keV, the detector resolution is 0.2808 and 0.243 keV respectively. The detector efficiency was determined using calibrated Am^{241} x-ray sources. For x-ray energies ranging from 6 to 20 keV, the efficiency approaches unity.

4 EXPERIMENTAL RESULTS

1. Laser-Compton spectra

Once a clear LCS signal was detected, a time scan was performed. The goal of this time scan was to optimize the LCS x-ray yield as a function of the delay between the electron beam and laser pulses. In order to remove possible pile up from the 7.5 keV x-ray resulting from the interaction of the electron beam with the 1064 nm laser line, a 25.4 μm thick stainless steel (SS) foil was placed in front of the Si(Li) detector. The x-ray transmission in air and SS foil for the 7.5 keV line was about 0.01% compared to 20% for the 15 keV line. Figure 3 shows the LCS signal as a function of the time delay between the electron beam and laser bunches. In these measurements the laser pulse length was equal to 7 ns, each point corresponds to an integrated yield from a LCS spectrum and the data collection time for each point was equal to 600 s. Figure 3 gives information on the electron bunch longitudinal distribution. One can also deduct from figure 3 an approximate value of the jitter between the electron beam and laser, for a 7ns long laser pulse and a 5 ns electron beam burst, the jitter is small and is of the order a ns. In the head-on collision geometry, this value of the jitter does not appear to be a severe limitation to observe LCS.

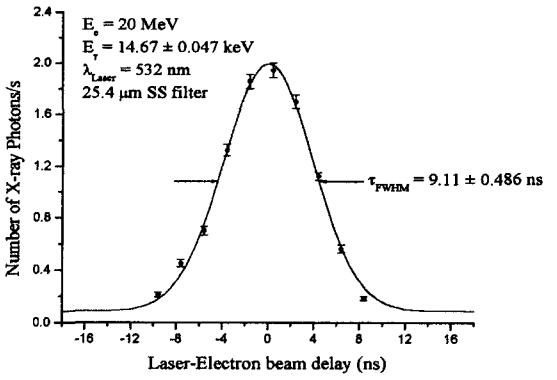

Figure 3. Time delay between laser and electron beam pulses. The curve was obtained using the x-rays generated from the interaction of the electron bunch and the 532 line of the Nd:YAG laser pulse.

Figure 4 shows the LCS spectrum for an observation angle equal to 3 mrad. The collection time for this spectrum was 600 s. The spectrum shows a clear sharp distinct monochromatic x-ray peak resulting from the interaction of the 20 MeV electron beam with the 532 nm laser line on top of a low bremsstrahlung background. The additional higher energy peak is due to pile up from the major line. The FWHM of the peak at 29.35 keV is about $\sqrt{2}$ larger than the width of the main peak, which is consistent with pileup.

Figure 5 shows the photon energies as a function of the electron beam energy for the second order LCS together with Eq. 2 for an emission angle of 3 mrad. There is good agreement between the data collected and the theoretical predictions. The

discrepancy observed for the electron energy equal to 22 MeV results from a change in the electron beam direction during beam tuning and therefore a change in the observation angle of the order of 5 mrad.

2. Laser-Compton energy spread

LCS energy spread depends on the energy spread of the laser, the electron beam energy and angular spread and the spread of the scattering angle subtended by the detector. The natural LCS spectral width is be given by:

$$\left(\Delta E_\gamma / E_\gamma\right)^2 = \left(\Delta E_L / E_L\right)^2 + \left(\Delta E_b^e / E_b^e\right)^2 + \left(2\Delta E_{Beam} / E_{Beam}\right)^2 + \left(\Delta E_\gamma^\theta / E_\gamma^\theta\right)^2 \quad (4),$$

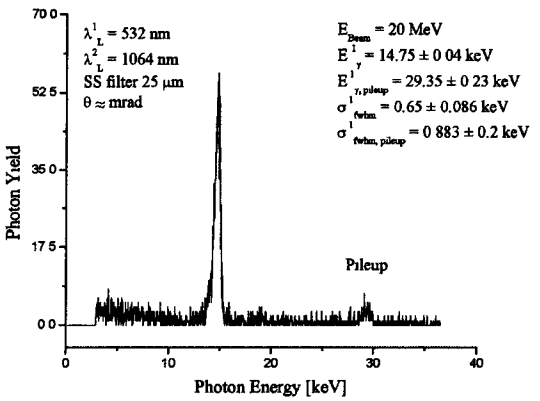

Figure 4. LCS spectrum using the Nd:YAG laser 532 line.

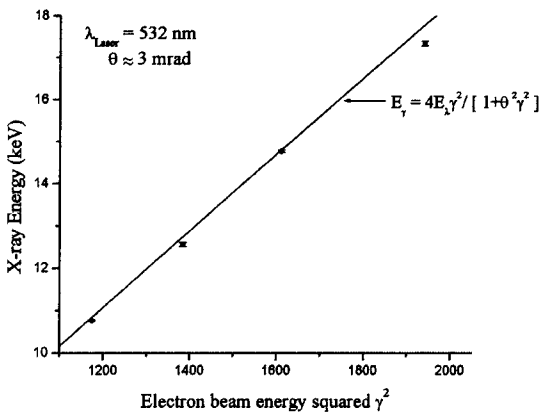

Figure 5. Second order LCS x-ray energy as a function of electron energy square.

where ΔE_L, ΔE_{Beam} correspond to the energy deviation of the laser and electron beam respectively and $\Delta E_L/E_L = 2.0\ 10^{-4}$ is negligible compared to $\Delta E_{Beam}/E_{Beam}$. ΔE_b^{ε} takes into account the electron beam angular spread. Because of the small solid angle, we have ignored the contribution to the energy resolution due to the finite collimation ΔE_γ^{θ} [9] in the LCS natural spectral width. The observed LCS energy spread ΔE_{Obs} is the quadradure sum of the LCS width and detector energy resolution given in Eq. 4. The LCS spectral width ΔE_γ is of the form:

$$\Delta E_\gamma^2 = \Delta E_{\mathrm{Obs}}^2 - \Gamma_{\mathrm{fwhm}}^2 \quad \text{(5a)},$$

The electron beam energy deviation is dominated by the width of the analyzing slits. The maximum electron beam current is recorded when the width of the slits is larger or equal to 3.5 cm. Figure 6 shows the variation of LCS energy spread (Eq. 5a) as a function of electron beam energy deviation for an observation angle θ equal to 3 mrad and x-ray energy equal to 14.75 keV, together with Eq. 5b given by:

$$\Delta E_\gamma = \frac{2E_\gamma \Delta E_{\mathrm{Beam}}}{\left[(E_{\mathrm{Beam}} + mc^2)(1+\gamma^2\theta^2)\right]} \quad \text{(5b)}.$$

The upper x-axis in Fig. 6 is the analyzing slits width and the lower x-axis is the corresponding electron beam energy spread. From this measurement, we see that the LCS width is solely determined by the electron beam energy deviation and that the contribution of electron beam angular spread is negligible.

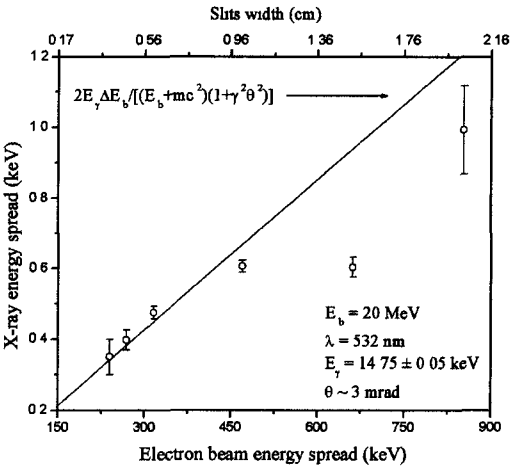

Figure 6. LCS natural energy spread as a function of the electron beam energy deviation. The electron beam energy spread was varied by changing the width of the 90° port slits [6]. The maximum slits width was about 5 cm.

There is good agreement between experimental and predicted values. As the widths of the electron beam slits are increased (larger than 0.9 cm) LCS energy spread reaches a maximum and a constant value as can be seen from figure 6.
There are two possible explanations for the constant value of LCS energy spread. Because the width of the slits also changes the size of the electron beam, we can conclude that the electron beam spot size becomes comparable to that of the laser when the maximum LCS energy spread is reached. Also, if we assume that the electron beam divergence is negligible because of the narrow slits' width, one sees that the maximum LCS energy spread equal to 0.6 keV corresponds (using eq. 5b) to a maximum electron energy spread equal to 420 keV. This value remains constant as the width of the slits is increased. Therefore, only electrons with an energy deviation $\Delta E_{beam} \leq 420$ keV are bent toward the interaction area [6]. Increasing the slits width above 0.9 cm would not affect the width of the Compton peaks but increase the electron beam current and spot size.
When the width of the slits is increased beyond 1.5 cm, the extra broadening of LCS width is mainly due the increase in bremsstrahlung background. The narrowest LCS width obtained is shown on figure 7. The width of the slit was set to optimize the signal to noise ratio and corresponds to an electron energy spread of 384 keV ($\Delta E_b / E_b \approx 2\%$). The electron beam was then tuned to reduce the electron beam phase angle spread. The width of the observed LCS spectral peak was equal to 0.397 keV. This corresponds, once the detector resolution is subtracted, to a width equal to 0.28 keV. From Eq. 5b, the electron beam energy spread was equal to 198.2 keV ($\Delta E_b / E_b \approx 1\%$).

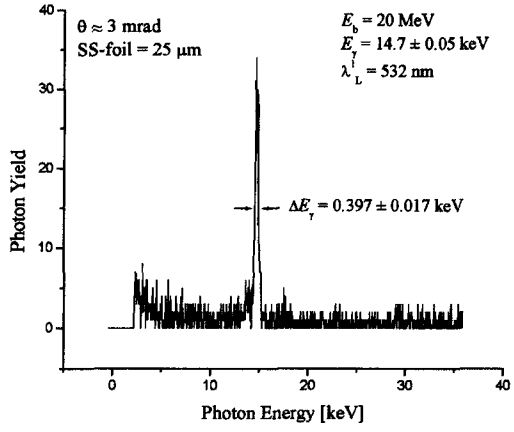

Figure 7. Narrowest line observed during the LCS experiment.

3. Angular distribution

During this experiment the electron beam was equal to 22 MeV and as before, only the Nd:YAG laser second harmonic was used. The x-rays travel through a 50.8 μm

thick, 4 inches in diameter stainless steel (SS) window and 0.5 m of air before they reach a Si-PIN Photodiode x-ray detector. The detector has an opening area equal to $7mm^2$ and was placed on translation stages for horizontal (x) and vertical (y) scans. Once the center of the x-ray cone is located (maximum x-ray energy in x and y directions) a finer scan is performed. Because the broadband mirror was close to the beam line axis, only results from the vertical scan are shown. Figure 8a shows the variation of the x-ray energy as a function of the vertical observation angle together with a fit using Eq. 1.

The cut-off angles correspond to the limit of the scan. The detector is aligned with the beam line axis when $\theta = 0$ mrad. Several observations can be made from Fig. 8a. One can see that the electron beam makes a vertical angle equal to 2.15 mrad with respect to the beam line axis and therefore by steering the electron beam down vertically the curve should shift to have its maximum at $\theta = 0$ mrad. The width of the curve, for a specific x-ray energy, gives the value of the distance between the detector and the interaction point, and its height is a direct measure of the electron beam energy. A fit to the data shows that electron beam energy is equal to 22.087 MeV and that the interaction point is located about 7.34 m from the x-ray detector. This will place the interaction point at the exit of the focusing quadrupoles. This value is consistent with

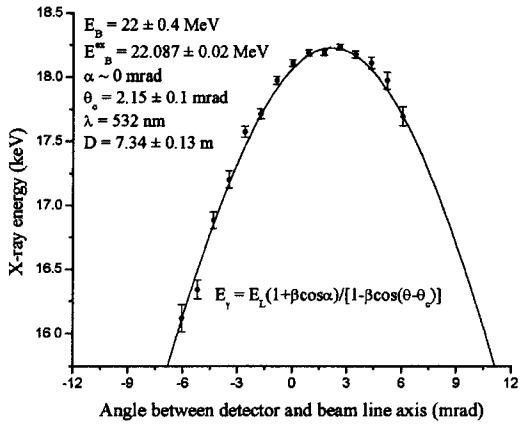

Figure 8a. Variation of LCS x-ray energy as a function of vertical observation angle. The SS windows blocks x-rays with angles greater and smaller than 6 and –6 mrad with respect to the beam line axis. Fit to the data provides values of the electron beam energy, distance from interaction point to detector and electron beam direction with respect to the beam line axis.

the time delay between the signal from the photomultiplier and the fast pickup beam monitor (Fig. 2).

The total number of LCS x-rays $N(\theta)$, as a function of the observation angle θ is given by:

$$N(\theta) = \iint_{\Delta\Omega_{det}} Abs(E_\gamma) \frac{d^2\sigma^{cv}}{d\theta_x d\theta_y} d\Omega \quad (6a),$$

$$\frac{d^2\sigma^{cv}}{d\theta_x d\theta_y} = \frac{d^2\sigma}{d\theta_x d\theta_y} \otimes g(\sigma_x, \sigma_y) \quad (6b).$$

$\Delta\Omega_{det}$ is the solid angle subtended by the detector. θ_x, θ_y are the horizontal and vertical photon directions respectively. $Abs(E_\gamma)$ is a function that takes into account the detector efficiency and the x-ray absorption in different media. $d^2\sigma^{cv}/d\theta x d\theta y$ is the convolution of the single photon differential cross section $d^2\sigma/d\theta x d\theta y$ for linearly polarized incident radiation [10], with the electron beam horizontal and vertical angular distribution $g(\sigma_x,\sigma_y)$ of RMS widths σ_x and σ_y respectively. Because of the large distance between the detector and interaction region, the stainless steal window as well as the distance in air enabled us the narrow the x-ray cone by absorption of the lower energy x-rays. The solid angle subtended by the detector was equal to $d\Omega_\gamma \approx 1.3x10^{-7}$ Sr, the width of the analyzing slits was equal to 1 cm and therefore about 25% of the total electron beam current was transmitted. At this slit's width, we believe that at the interaction, the electron beam spot size is larger than that of the laser and that the electron beam divergence is not negligible. Figure 8b shows the variation of the x-ray intensity as a function of the vertical observation angle (angle between the beam line axis and detector), together with the fit to the data with a reduced $\chi^2 \approx 3.25$. The normalization of the spectra was done by measuring the current from the fast toroid. With the current number and quality of the data collected (due to beam current and laser power fluctuations), it is difficult to obtain an accurate measurement of the electron beam divergence.

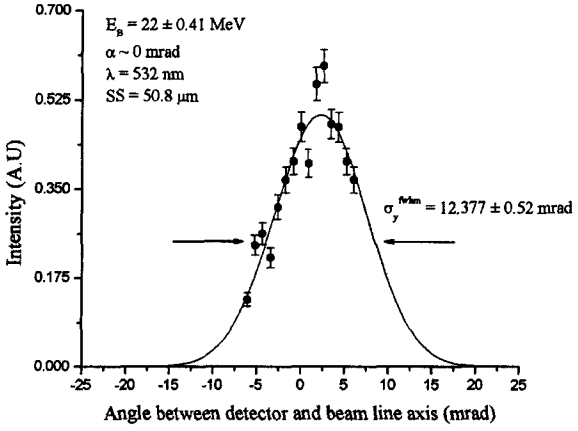

Figure 8b. Intensity as a function of observation angle, together with the fit to the data using Eq. 6a. The x-rays travel through a 50.8 μm thick window and 0.5 m in air before they reach the detector.

The vertical RMS σ_y = 3.54 mrad, previously measured using OTR [6] was obtained at a position located 1.2 m downstream from the interaction point and for a slits width greater than 3.5 cm.

5 CONCLUSION

LCS x-ray peaks resulting from the head-on interaction of a Nd:YAG laser and a 20-22 MeV electron beam were observed during our experiments at the IAC. We have shown that there is a good agreement between experiment and theoretical predictions. We have also demonstrated the direct relation between measured LCS width and electron beam energy deviation. This suggests that LCS could provide an excellent probe of electron beam energy and energy spread. We have also shown that although LCS can be viewed as a potential bright x-ray source, it can also provide valuable information on the longitudinal electron beam distribution, beam energy and direction with respect the electron beam line. By placing an array or arrays of Si-PIN detectors at the x-ray port and an appropriate data acquisition system, it is possible to have an online beam monitoring system.

ACKNOWLEDGMENT

This work partially funded by US Department of Energy under DOE Idaho Operations Office Contract Number DE-AC07-99ID13727.

REFERENCES

[1] W. P. Leemans et al., Phys. Rev. Lett. 77 (1996) 4182.
[2] T. Shintake, Nucl. Instr. and Meth A 311 (1992) 453.
[3] I. C. Hsu et al. Phys. Rev. E 54 (1996) 5657.
[4] G. Ya. Kezerashvili et al. Nucl. Instr. and Meth. B 145 (1998) 43.
[5] I. V. Pogorelsky et al., Nucl. Instr. and Meth. A 455 (2000) 176.
[6] K. Chouffani et al., to be published in Nucl. Instr. And Meth. A
[7] E. Esarey et al., Nucl. Instr. and Meth. A 331 (1993) 545.
[8] R. Fiorito, private communication.
[9] G. Matone et al. in "*Lecture Notes in Physics*", S. Costa and C. Schaerf (Eds), Springer-Verlag, Berlin, 1976.
[10] J. D. Jakson, Classical Electrodynamics, 2nd ed. (Wiley, New York, 1975)